Boletim da Sociedade Astronômica Brasileira, **37**, no. 1, 310-314

A millimetric survey of AGN + Sgr A* with ALMA

Spectropolarimetric properties and their evolution between 2017 and 2023

D. Carlos[1] & C. Goddi[1,2,3,4]

[1] Instituto de Astronomia, Geofísica e Ciências Atmosféricas, Universidade de São Paulo, São Paulo, SP, 05508-090, Brazil e-mail: douglas.carlos@usp.br
[2] Dipartimento di Fisica, Università degli Studi di Cagliari, SP Monserrato-Sestu km 0.7, I-09042 Monserrato, Italy e-mail: cgoddi@usp.br
[3] INAF - Osservatorio Astronomico di Cagliari, via della Scienza 5, I-09047 Selargius (CA), Italy
[4] INFN, Sezione di Cagliari, Cittadella Univ., I-09042 Monserrato (CA), Italy

Abstract. We present a survey of the spectropolarimetric properties of a sample of AGN and Sgr A* observed with the Atacama Large Millimeter/submillimeter Array (ALMA), over five VLBI campaigns conducted from 2017 to 2023. We perform a comprehensive characterization of the compact cores in total intensity and polarization, investigating the trends of the linear polarization fraction (LP), the electric vector position angle (EVPA), and rotation measure (RM). The analysis includes both time-domain and spectral-domain, allowing us to track the variability of each source on weekly and annual timescales, and to compare their behavior across millimeter/submillimeter wavelengths.

Resumo. Apresentamos um levantamento das propriedades espectropolarimétricas de uma amostra de AGN e Sgr A* observada com o Atacama Large Millimeter/submillimeter Array (ALMA), ao longo de cinco campanhas de VLBI realizadas de 2017 a 2023. Realizamos uma caracterização completa dos núcleos compactos em intensidade total e polarização, investigando as tendências da fração de polarização linear (LP), o ângulo de posição do vetor elétrico (EVPA) e medida de rotação (RM). A análise inclui tanto o domínio temporal quanto espectral, permitindo-nos rastrear a variabilidade de cada fonte em escalas de tempo semanais e anuais, e comparar seu comportamento em comprimentos de onda milimétricos/submilímetro.

Keywords. Galaxies: active – Galaxies: jets – Galaxy: nucleus

1. Introduction

The polarization of synchrotron radiation in active galactic nuclei (AGN) serves as a powerful probe of both the emission region near the central supermassive black hole and the surrounding magnetoionic environment through which it propagates. The polarization properties of the radiation, such as the degree of polarization and the orientation of the electric vector position angle (EVPA), carry information about the structure and degree of order of the magnetic field in the emitting region (Asada et al. 2002; Gabuzda et al. 2006). Changes in these properties over time and frequency also provide constraints on the size, geometry, and dynamical behavior of the emission region, such as shock propagation, changes in jet orientation, or the ejection of new VLBI components (Pacholczyk 1970; Hughes et al. 1989; Pohl et al. 1995; Jorstad et al. 2001).

However, plasma effects and uncertainties about the flow kinematics and composition make it difficult to directly relate the observed EVPA to the field properties at the source. There is the Faraday effect, for instance, in which the polarized radiation traversing a magnetized plasma will have its EVPA rotated by an amount proportional to the rotation measure (RM):

$$\mathrm{RM} = 8.1 \times 10^5 \int n_e B_{\parallel} \cdot dl \quad \mathrm{rad\ m^{-2}} \tag{1}$$

where n_e is the electron number density of the medium (in $\mathrm{cm^{-3}}$), $B_{\parallel}$ is the component of the magnetic field parallel to our line of sight (in G), and l is the path of a photon through the plasma towards the observer (in pc). This magnetized medium is called the "Faraday screen". Monitoring the polarization properties of AGN across multiple spectral bands and over different timescales provides a powerful diagnostic of both the synchrotron-emitting region and the intervening Faraday screen.

The Atacama Large Millimeter/submillimeter Array (ALMA) offers a uniquely powerful platform for studying the polarization properties of AGN, due to its combination of high sensitivity, wide frequency coverage, and spatial resolution at mm and sub-mm wavelengths. Furthermore, the inclusion of ALMA as a phased-array element Goddi et al. (2019) in global very long baseline interferometry (VLBI) networks such as the Global-mm VLBI Array (GMVA, Martí-Vidal et al. 2012) and the Event Horizon Telescope (EHT, EHTC 2019b), has contributed critical sensitivity to long-baseline observations. This has culminated in landmark results like the imaging the shadows of the supermassive black holes M87* (EHTC 2019a) and Sgr A* (EHTC 2022), among others. Such observations are essential for testing theoretical models of jet launching such as Blandford & Znajek (1977) and Blandford & Königl (1979).

With this in mind, we started VAPOLA—the first online, multi-epoch, multi-band repository of high-level data products from ALMA observations of AGN and Sgr A* during VLBI global campaigns. The high-level products are obtained by running an automated pipeline that processes fully calibrated ALMA data, following the procedures outlined in Goddi (2021); Goddi & Carlos (2025) and standardized in Mus et al. (in prep)[hereafter, VAPOLA I]. This study represents the first scientific exploration of the high-level products from the VAPOLA archive, where we analyze the spectropolarimetric properties of a sample of 39 AGNs and Sgr A*, observed with ALMA during five VLBI campaigns spanning 2017 to 2023. We perform a comprehensive characterization of the compact cores in total intensity and polarization.

2. Observations and sample

The data we present were acquired with the ALMA observatory during the VLBI campaigns conducted by the GMVA and the EHT in 2017, 2018, 2021, 2022 and 2023, as part of ALMA Cycles 4, 5, 7, 8 and 9 respectively. These consist of non-simultaneous but close in time observations performed at ALMA Band 3 (B3, λ3 mm or 93.3 GHz) with the GMVA, and Band 6 (B6, λ1.3 mm or 221.1 GHz) and Band 7 (B7, λ0.87mm or 342.6 GHz) with the EHT, of a variety of objects, during one to two weeks each year, either in April or March.

The 39 objects in the sample consist of 29 quasars, 9 radiogalaxies, and the strong radio source at the Galactic Center (GS), Sgr A*. Of the quasars, 21 are FSRQs, 7 are BL Lacs, and one has unknown optical classification. The active galaxies class includes mainly radio galaxies such as M87, Centaurus A (Cen A), M84, 3C84, NGC4261, and also low luminosity AGN like NGC1052, NGC4594, NGC4278 and NGC5232.

3. Methods

We produced full-Stokes images of every source to allow for the study of extended sources. These include maps of Stokes I, linear polarization fraction (LP) and electric field vector position angle (EVPA, or χ). Figure 1 shows example for the kpc jet of the M87 galaxy.

By fitting a point source model to the phase center of the visibilities using the external CASA library UVMULTIFIT (Martí-Vidal et al. 2014), we extract the Stokes parameters of the compact cores. We assume the emission is dominated by the compact core and run UVMULTIFIT to fit a delta function at the phase center of the sources, obtaining their Stokes parameters at each SPW for all bands. The Stokes parameters can then be combined to describe the polarization characteristic of the sources at the observed frequencies.

The LP and EVPA are obtained directly from Stokes Q and U in each SPW, as shown in Equations 2 and 3 respectively. The errors of the Stokes parameters per SPW are estimated from simple propagation of uncertainties, combining the root mean squared errors (RMS) terms with the 3% leakage term of Stokes I onto Q and U summed in quadrature, as is recommended by the ALMA observatory.

$$\mathrm{LP} = \sqrt{Q^2 + U^2}/I \tag{2}$$

$$\chi = \frac{1}{2}\arctan\left(\frac{U}{Q}\right) \tag{3}$$

The depolarization D and the Faraday rotation measure RM are obtained from the spectral behavior of LP and EVPAs respectively. This consists of simple least-squares linear fits to the said quantities over the SPWs of each band. For RM, we fit the EVPAs as a function of λ^2, while D is obtained from the derivative of LP, as shown in Equation 4:

$$D = \frac{d}{d\nu} LP \tag{4}$$

The depolarization is interesting because, like the RM, it can also carry information about the medium surrounding the source. If the Faraday screen medium can be described as a simple external screen with a coherent magnetic field, we should expect a simple rotation of the EVPAs at all wavelengths, but no depolarization should occur ($D = 0$). The presence of irregularities in the screen can lead to the depolarization of the longer wavelengths ($D > 0$), as these are more strongly affected by the Faraday effect (Burn 1966; Tribble 1991). This effect is called Faraday dispersion or beam depolarization. It is also possible to observe $D < 0$, which means that the polarization of the source is larger for longer wavelengths. This is called anomalous depolarization or inverse depolarization (Sokoloff et al. 1998; Homan 2012), and it cannot be described by a simple external screen model; if one encounters $D < 0$ it is necessary to consider different depolarization models, such as multiple Faraday components or even internal Faraday rotation.
The VAPOLA archive includes observations performed in three different ALMA bands, and some of the sources are observed in more than one band during the same week. By combining the data from the different bands, it is possible to study the behavior of the polarimetric properties of the cores over the mm to sub-mm wavelength range. As an example, we summarize the interband spectropolarimetric properties of quasar 3C273 by plotting its spectrum (Stokes I vs. ν), linear polarization (LP vs. ν), and Faraday rotation (χ vs. λ^2) in Figures 2.

As the data presented here encompass one or two weeks of observation from each year, they allow us to study how variable the sources are on weekly and yearly timescales. The ALMA Compact Array regularly monitors many bright sources as part of the Grid-survey (GS). This survey mainly targets quasars and BL Lacs that span the entire range of R.A., which are observed in full-polarization mode, along with solar system objects for calibration purposes (AMAPOLA[1]). The evolution of AMAPOLA measurements (I, LP and EVPA) covering the period 2016-2025 is plotted in Figure 3 for the subgroup of the most observed sources during the VLBI campaigns, where we have binned the data into 7-day intervals.

4. Differences between object classes

By making use of the available ALMA measurements from all years, we can study the distributions of the mm and sub-mm emission properties as a function of source class.

BL Lacs are more polarized, and their polarization fractions (8.0 ± 3.6)% cover a wider range than those of FSRQs with LP = (2.7 ± 2.7)% The LP of FSRQs also does not seem to grow with frequency as much as the other classes. The median depolarization of FSRQs $(0.31 \pm 1.97) \times 10^{-4}$ GHz^{-1} is much lower than that of BL Lacs $(1.46 \pm 1.29) \times 10^{-4}$ GHz^{-1}, owing to the fact that the former exhibits episodes of inverse depolarization much more often than the latter. Both the median and the scatter of $|\mathrm{RM}|_{\mathrm{rest}}$ are larger for FSRQs $(1.34 \pm 2.80) \times 10^5$ rad/m^2 than for BL Lacs $(0.68 \pm 2.21) \times 10^5$ rad/m^2, and both classes show evidence of $|\mathrm{RM}|_{\mathrm{rest}}$ increasing with frequency.

The active galaxies are much less polarized than quasars, showing a median and scatter of only (1.2 ± 0.9)%; the highest recorded LP comes from M87, with 2.8% at 343 GHz in 2021. In terms of depolarization, galaxies have larger $D = (1.81 \pm 1.75) \times 10^{-4}$ GHz^{-1} than BL Lacs. The $|\mathrm{RM}|_{\mathrm{rest}}$ distribution of galaxies has a larger median than that of quasars, but a similar spread, with $(2.33 \pm 1.91) \times 10^5$ rad/m^2.

The LP of Sgr A* (4.4 ± 2.4)% is, on average, higher than that of active galaxies and FSRQs, with a similarly large spread; at 343 GHz, the LP can reach values as high as those of BL Lacs (8.8%). The median depolarization is also greater than that of other classes $(3.41 \pm 2.05) \times 10^{-4}$ GHz^{-1} , and is larger

[1] https://www.alma.cl/~skameno/AMAPOLA/

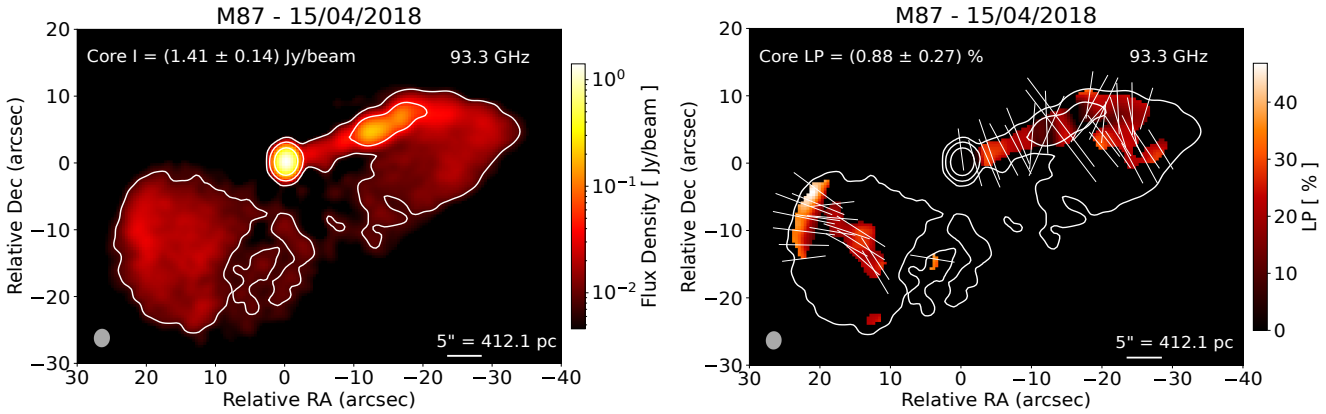

Figure 1. Jet images of M87 at 93 GHz. Left: Stokes I maps. Right: linear polarization (LP) fraction maps with EVPA orientation overlaid on top, the length of the EVPA lines are proportional to polarized flux. The images include contours starting at 5×RMS of Stokes I (1.12 mJy) and the beam dimensions are 2.61" × 2.13" (−4.0°).

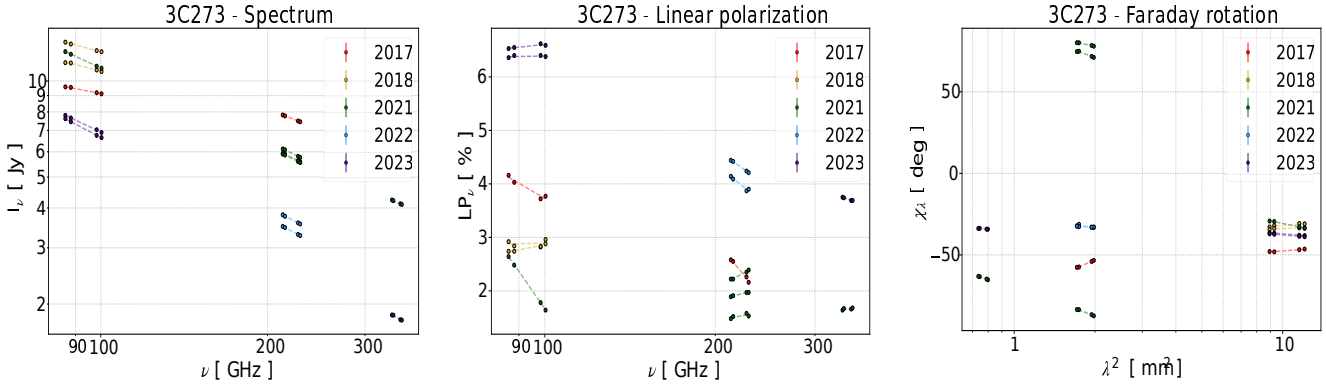

Figure 2. Spectral distribution of Stokes I (left), LP (center) and EVPA (right) for 3C273. In all panels, different color and shapes represent different years and observing modes (circle: VLBI, triangle: non-VLBI) respectively.

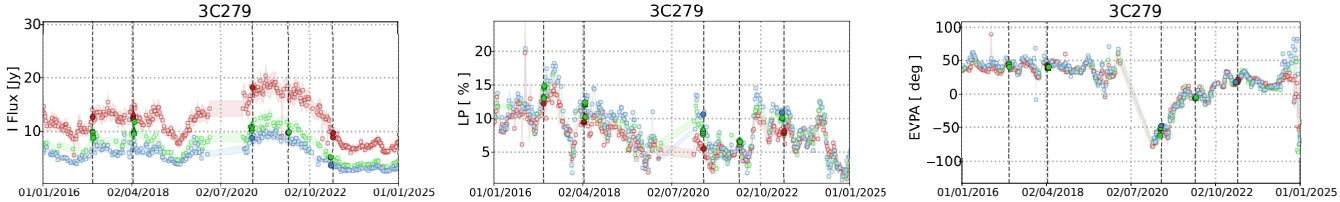

Figure 3. VLBI+AMAPOLA measurements for 3C279 in the 2016-2025 period. Each column represents different parameters; Left: Stokes I, Center: LP, Right: EVPA. The different colors represent different bands; red: 98 GHz, green: 230 GHz, cyan: 343 GHz. The vertical black dashed lines indicate the date of the VLBI campaigns.

for the lower frequencies. Sgr A* has never shown inverse depolarization. Unlike other objects, all measurements available so far show a consistently negative RM for Sgr A* of around $(-5.11 \pm 1.98) \times 10^5$ rad/m^2, which is likely the result of a stable magnetic field configuration in the Faraday screen. Furthermore, its RM magnitude also clearly scales with frequency.

5. Discussion

The data we present is well-suited for performing polarization modeling of our SMBH targets. We explore the simplest possible model that can still account for cases of regular depolarization observed in the narrow-band ALMA observations.

According to Burn (1966), the presence of a turbulent magnetic field in an external Faraday screen can cause beam depolarization if the coherence length scale of the magnetic field at the source is smaller than the telescope beam. This Burn-type depolarization takes the form of an exponential drop-off as shown in Equation 5, where LP_0 is the intrinsic linear polarization fraction and $\sigma_{\rm RM}$ is the Gaussian variance of RM from the incoherent magnetic field, which is called the RM dispersion (Fanti et al. 2004; Farnsworth et al. 2011; Pasetto 2021).

$$LP(\lambda) = LP_0 e^{-2\sigma_{RM}^2 \lambda^4} \quad (5)$$

From this, one can take the derivative with respect to the frequency ν to obtain $\sigma_{\rm RM}$ directly from the measured depolarization D and LP as shown in Equation 6:

$$\sigma_{\rm RM} = \sqrt{\frac{\nu^5 D(\nu)}{8c^4 LP(\nu)}} \tag{6}$$

Note how this model is incapable of explaining inverse depolarization, since $D(\nu) < 0$ would imply a non-real $\sigma_{\rm RM}$. We calculate $\sigma^{\rm rest}_{\rm RM} = (1+z)^2\sigma_{\rm RM}$ for all instances where positive depolarization was measured, completely ignoring sources that most frequently display inverse depolarization (3C273 and J1744-3116).

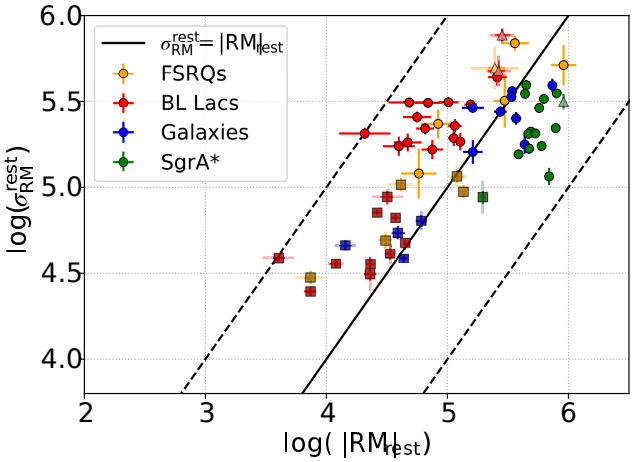

Figure 4. Rest-frame RM dispersion $\sigma^{\rm rest}_{\rm RM}$ as a function of rest-frame RM magnitude . The solid line represents $\sigma^{\rm rest}_{\rm RM} = |{\rm RM}|_{\rm rest}$ case, while the top and bottom dashed lines stand for $\sigma^{\rm rest}_{\rm RM} = 0.1|{\rm RM}|_{\rm rest}$ and $\sigma^{\rm rest}_{\rm RM} = 10|{\rm RM}|_{\rm rest}$ for comparison. The four main colors (yellow, red, blue, green and pink) are used to distinguish between the classes (FSRQs, BL Lacs, active galaxies, Sgr A* and unknown), while different shapes and shades represent measurements at different bands (darker squares, circles and lighter triangles for 93, 221 and 343 GHz, respectively).

Figure 4 illustrates how the rest-frame RM dispersion $\sigma^{\rm rest}_{\rm RM}$ increases with frequency for all classes, together with $|{\rm RM}|^{\rm rest}$. The frequency dependence of $\sigma^{\rm rest}_{\rm RM}$ implies that this simple model of Burn-like depolarization is unfit to describe the full wavelength range. In any case, we can still gain some insight into the multi-band polarization behavior of the sources using this model by noting that, in Equation 5, a smaller $\sigma_{\rm RM}$ at lower frequencies means the source depolarizes more slowly with increasing wavelength. We found a power law trend $\sigma^{\rm rest}_{\rm RM} \propto (|{\rm RM}|_{\rm rest})^{\gamma}$ with similar indices when we fit each class separately; quasars (FSRQs+BL Lacs) have $\gamma = 0.67 \pm 0.08$, with a significance score of 5.5σ, active galaxies have $\gamma = 0.7 \pm 0.10$ with 3.6σ, and SgrA* shows $\gamma = 0.38 \pm 0.31$ with a low significance of only 1σ even after excluding potential outliers. These similarities support the idea that the strength of the turbulent depolarizing field scales with that of the Faraday rotating field. This is very unexpected since, in Burn-like depolarization laws, $\sigma_{\rm RM}$ and RM are treated as two independent free parameters. Interestingly, although the different classes have similar values of RM dispersion, if we consider the ratio $r = \sigma^{\rm rest}_{\rm RM}/|{\rm RM}|_{\rm rest}$ for all bands, we will notice that quasars are characterized by

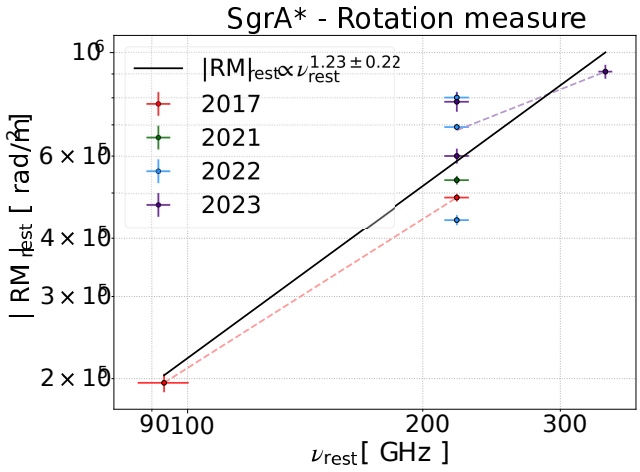

Figure 5. Plot of |RM| as a function of frequency for SgrA*. The black solid line represents the fit using all data, while the colored dashed lines represent fitting using data from specific years.

$r = 1.9 \pm 1.0$, while galaxies have $r = 1.0 \pm 0.7$ and Sgr A* has $r = 0.43 \pm 0.18$ (the scatter becomes 2.8 if we include very low RM episodes. If the $\sigma^{\rm rest}_{\rm RM}/|{\rm RM}|_{\rm rest}$ ratio is a good proxy for the strength of the turbulent field relative to the coherent field (as suggested by Rossetti et al. 2008), then the polarization properties of quasars could have a larger contribution from the turbulent component than those of active galaxies and Sgr A*.

The Faraday RM is sensitive to the density of the medium traversed by the radiation and its magnetic field, following Equation 1. As the synchrotron opacity decreases with increasing frequency (Lobanov 1998), it is likely that observations from different bands will probe regions with different structure, with the highest frequencies arising from the innermost regions, where both the density and magnetic field strength are presumably higher. Using certain assumptions, Jorstad et al. (2007) derived that the magnitude of the RM should scale with the observing frequency as a power-law $|{\rm RM}| \propto \nu^a$. Since we have observations from multiple ALMA bands, we checked the dependence of $|{\rm RM}|_{\rm rest}$ on $\nu_{\rm rest} = (1+z)\nu$ for our best-covered sources and investigated what this may tell us about their jet geometry. To do this, we included all tentative (SNR> 2) measurements for each source and performed a simple fit to obtain the power-law index $a_{\rm all}$.

If the connection of a to the jet geometry is true, these results would point to the presence of very collimated outflows in Sgr A*. Alternatively, Li et al. (2015) determined that the jet model presented in Falcke & Markoff (2000) alone is insufficient to reproduce the high observed RM of Sgr A*, and that the accretion flow can have a significant contribution under specific conditions. If the accretion flow itself can act as the Faraday screen, as suggested by Marrone et al. (2006) and GRMHD simulations (Ricarte et al. 2020; Ressler et al. 2023), then we could still expect to see the RM magnitude increase with frequency due to the aforementioned opacity effects. This exercise illustrates how a power-law dependence of RM with frequency is not a unique consequence of jet models.

6. Conclusions

We have presented ALMA observations of several AGN + SgrA* performed during the VLBI campaigns of the GMVA and EHT

from 2017 to 2023. The observations cover a few days across one to two weeks each year and include data from three bands, allowing us to determine the spectral and polarimetric behavior of the target sources in the 88 – 345 GHz (0.87 – 3.4 mm) range. Among the 39 targets, there are 29 quasars (22 FSRQs, 7 BL Lacs, 1 unknown), 9 active galaxies, and Sgr A*. We analyze the subset of the most well-covered sources in detail and report the observed trends in their spectral and polarimetric properties over the 2017-2023 interval. Our main findings include:

- Sources are generally stable in flux and spectra within weekly timescales but can change depending on the year. Short-term polarization variability is more common, and we sometimes observe sudden changes in both polarization fractions and EVPAs from one day to the next.
- When the polarization changes occur during flaring states, they could be associated with the evolution of jet components unresolved by ALMA. This hypothesis can be verified in the future using VLBI data acquired during the same period and beyond.
- Of the quasars, the BL Lacs are more polarized at mm/sub-mm wavelengths than FSRQs. Active galaxies are much less polarized than quasars, but they are also less polarized than Sgr A*, which can reach LPs of almost 9% at 343 GHz, similar to those measured for BL Lacs.
- The majority of sources have a polarization profile that increases with frequency. The FSRQ class includes almost all of the counterexamples, displaying as many episodes of inverse depolarization as regular polarization. 3C273 is the source that most frequently displays inverse depolarization, including in its quiescent state, pointing to the presence of lasting complex Faraday structures. Detailed modeling and a wide wavelength coverage are needed to constrain the properties of such structures.
- The relatively high RM values obtained ($\sim 10^4 - 10^5$ rad/m^2) suggest ordered, large-scale magnetic field structures close to the central object. These are usually stable during the same observing week but can change sign and magnitude on timescales of a few years. Sgr A*, on the other hand, has a consistently negative RM; however, on two occasions, its RM magnitude dropped significantly from one day to the next during episodes of fast-changing polarization before returning to the same level as the previous day. The variable character of the RM in Sgr A* and other sources could hint at the dynamical nature of the Faraday screen.
- We studied the cases of regular depolarization in the narrow-band data by assuming that it occurs due to a turbulent Faraday screen. The resulting rest-frame RM dispersions $\sigma_{\rm RM}^{\rm rest}$ increase with frequency for all classes, which means the polarization fraction decreases more slowly for longer wavelengths. We discuss the possibility that opacity effects, which are generally not taken into account in analytical polarization models from the literature, could be responsible for the frequency behavior.
- We found that both quasars and active galaxies display a correlation between $\sigma_{\rm RM}^{\rm rest}$ and $|{\rm RM}|_{\rm rest}$. This may mean that the strength of the turbulent component of the magnetic field scales with that of the ordered component in the Faraday screen. SgrA* has the lowest $\sigma_{\rm RM}^{\rm rest}/|{\rm RM}|_{\rm rest}$ ratio, which we argue could be associated with its long-term RM stability.
- Using observations from the three ALMA bands, we find evidence of a power-law dependence of |RM| with frequency, with indices in the range of $a \sim 0.7 - 4.4$. These values are consistent with the RM arising in a magnetized sheath layer surrounding the relativistic jet, allowing us to place constraints on the jet geometry. An alternative interpretation involves the accretion flow itself serving as the Faraday screen and cannot be excluded. This is especially relevant for Sgr A*, which does not have a confirmed jet.

Acknowledgements. We acknowledge support from the Coordenação de Aperfeiçoamento de Pessoal de Nível Superior (CAPES) of Brazil through PROEX grant number 88887.845378/2023-00

References

Asada, K., Inoue, M., Uchida, Y., et al. 2002, PASJ, 54, L39
Blandford, R. D. & Königl, A. 1979, ApJ, 232, 34
Blandford, R. D. & Znajek, R. L. 1977, MNRAS, 179, 433
Burn, B. J. 1966, MNRAS, 133, 67
Event Horizon Telescope Collaboration. 2019a, ApJL, 875, L1
Event Horizon Telescope Collaboration. 2019b, ApJL, 875, L2
Event Horizon Telescope Collaboration. 2022, ApJL, 930, L12
Falcke, H. & Markoff, S. 2000, A&A, 362, 113
Fanti, C., Branchesi, M., Cotton, W. D., et al. 2004, A&A, 427, 465
Farnsworth, D., Rudnick, L., & Brown, S. 2011, AJ, 141, 191
Gabuzda, D. C., Rastorgueva, E. A., Smith, P. S., & O'Sullivan, S. P. 2006, MNRAS, 369, 1596
Goddi, C., Martí-Vidal, I., Messias, H., et al. 2019, PASP, 131, 075003
Goddi, C. 2021, ApJL, 910, L14
Goddi, C. & Carlos, D. 2025, A&A, 699, A265
Homan, D. C. 2012, ApJL, 747, L24
Hughes, P. A., Aller, H. D., & Aller, M. F. 1989, ApJ, 341, 68
Jorstad, S. G., Marscher, A. P., Mattox, J. R., et al. 2001, ApJ, 556, 738
Jorstad, S. G., Marscher, A. P., Stevens, J. A., et al. 2007, AJ, 134, 799
Li, Y.-P., Yuan, F., & Wang, Q. D. 2015, ApJ, 798, 22
Lobanov, A. P. 1998, A&A, 330, 79
Marrone, D. P., Moran, J. M., Zhao, J.-H., & Rao, R. 2006, ApJ, 640, 308
Martí-Vidal, I., Krichbaum, T. P., Marscher, A., et al. 2012, A&A, 542, A107
Martí-Vidal, I., Vlemmings, W. H. T., Muller, S., & Casey, S. 2014, A&A, 563, A136
Pacholczyk, A. G. 1970, Radio Astrophysics, Freeman & Co.
Pasetto, A. 2021, Galaxies, 9, 56
Pohl, M., Reich, W., Krichbaum, T. P., et al. 1995, A&A, 303, 383
Ressler, S. M., White, C. J., & Quataert, E. 2023, MNRAS, 521, 4277
Ricarte, A., Prather, B. S., Wong, G. N., et al. 2020, MNRAS, 498, 5468
Rossetti, A., Dallacasa, D., Fanti, C., et al. 2008, A&A, 487, 865
Sokoloff, D. D., Bykov, A. A., Shukurov, A., et al. 1998, MNRAS, 299, 189
Tribble, P. C. 1991, MNRAS, 250, 726